Optics Communications 494 (2021) 127052

Contents lists available at ScienceDirect

Optics Communications

journal homepage: www.elsevier.com/locate/optcom

Role of the modal composition of pump in the multi-peak Brillouin gain spectrum in a few-mode fiber

Suchita [a,*], Balaji Srinivasan [a], Govind P. Agrawal [b], Deepa Venkitesh [a]

[a] Department of Electrical Engineering, Indian Institute of Technology Madras, Chennai 600036, India
[b] The Institute of Optics, University of Rochester, NY 14627, USA

ARTICLE INFO

Keywords:
Graded-index few mode fiber
Intramodal & Intermodal stimulated Brillouin scattering
Multi-peak Brillouin gain spectrum
Composite modes

ABSTRACT

We study stimulated Brillouin scattering (SBS) in a few-mode graded-index fiber in both the intermodal and intramodal configurations. A multi-peak Brillouin gain spectrum (BGS) is observed in both types of SBS interactions owing to the presence of higher-order acoustic modes, whose contribution to the Brillouin gain is found to depend on the modal composition of the pump beam. The numerically simulated results match well with the experimentally observed multi-peak BGS in both the intramodal and intermodal cases. The linewidth of the individual BGS peaks are extracted from a multi-Lorentzian fit to the data and are found to be significantly different for different modal compositions of the pump beam.

1. Introduction

Stimulated Brillouin scattering (SBS) is a nonlinear process that generates Stokes waves whose frequencies are downshifted due to the interaction of a narrowband optical pump radiation with hypersonic acoustic phonons of the medium. SBS is widely studied in single mode fibers (SMF) [1–4], where the buildup of Stokes radiation eventually limits the power that can be launched into a fiber, a feature of considerable concern especially in optical communication systems [5–7]. SBS has also been one of the primary deterrents to power scaling in high-power fiber amplifiers [8]. This issue is typically addressed by manipulating the spectrum of the input light and/or by using large mode area fibers [7]. Manipulation of dopant profiles to achieve the desired acoustic properties has also been reported [9,10]. The effective indices of supported optical modes and acoustic modes of the fiber determine the Brillouin frequency shift (BFS) values, which are entirely governed by the refractive index and the dopant profile of the fiber. The BFS and the spectral width of the Brillouin gain spectrum (BGS) are sensitive to the temperature and strain experienced by the fiber, which makes the accurate measurement of BGS extremely useful for sensing applications. Several variants of distributed sensors using SBS in an optical fiber have been demonstrated [11–13]. The BGS of an optical fiber can be calculated numerically for any specific fiber design by analyzing the modal overlap of the various optical and acoustic modes [14].

In addition to single mode fibers, few-mode fibers (FMFs) have also been used in recent years for distributed Brillouin sensing [15–17]. Their BGS is found to exhibit a multi-peak structure. Single mode fibers can also exhibit a multi-peak structure because of the interaction of the fundamental optical mode with multiple acoustic modes [18,19]. In contrast, higher-order optical modes are also involved in the case of FMFs. In both cases, such multi-peak structures are useful for sensing applications. The temperature/strain coefficients would be different for each of these peaks, and hence these multiple peaks in FMF have been used for the discrimination of temperature and strain during the sensing process [17]. Extensive theoretical as well as experimental studies on intermodal and intramodal SBS have been carried out to determine the Brillouin thresholds and linewidth characteristics [20–23]. The exact frequency of BFS peak is decided by the overlap of the corresponding optical and acoustic modes, which in turn depends on the dopant profiles. Numerical and experimental studies have also been done in the past for ascertaining the BGS of specialty fibers such as ring core fibers, micro-structured fibers, and polarization maintaining fibers [22,24,25]. Most of these studies are based on the characterization of the multi-peak BGS for intramodal and intermodal interactions with the higher-order acoustic modes for the purpose of a multi-parameter distributed fiber sensor. Apart from the intramodal and intermodal interactions with various acoustic modes, the multipeak BGS can be controlled by the mode composition of the pump and Stokes pair [22]. These studies are based on the externally excited probe mode configuration which is useful to study the externally stimulated Brillouin scattering. In this work, we launch the composite pump mode without injecting any external probe. In this case spontaneous SBS helps in generating the Stokes wave. We call this process in this paper a self-stimulating Brillouin process. Stokes generated from the spontaneous process from the farther end of the fiber starts getting amplified in the

* Corresponding author.
E-mail addresses: suchitay102@gmail.com (Suchita), deepa@ee.iitm.ac.in (D. Venkitesh).

https://doi.org/10.1016/j.optcom.2021.127052
Received 12 February 2021; Received in revised form 13 April 2021; Accepted 20 April 2021
Available online 22 April 2021

presence of the pump and results in a relatively strong signal which in turn triggers the stimulated Brillouin scattering process beyond the threshold pump power. The modal composition of pump and the supported acoustic modes control the SBS process in our case.

We focus our study on the role of modal composition of the input pump in deciding the interacting acoustic modes and hence the BGS in a graded-index (GI) FMF. We present a detailed study of the SBS characteristics of a graded-index FMF supporting three spatial modes. We carefully evaluate the supported optical and acoustic modes by this fiber and numerically find the BGS by considering all phase-matched intramodal and intermodal interactions occurring inside in a 1 km long FMF. We further measure the BGS experimentally for this fiber and map the multipeak structure to the specific acousto-optic mode interactions. We also identify the role of composition of the pump mode in deciding the nature of BFS. Section 2 focuses on the theory of SBS, including details of the acousto-optic mode solver and calculation of BGS. Section 3 explains the experimental details of intramodal and intermodal BGS measurements. In Section 4, we compare the experimental results with our numerical simulations. Section 5 presents the main conclusions of this study.

2. Numerical simulations of BGS in FMFs

In this section, we present our numerical model for the intramodal and intermodal Brillouin interactions. The objective is to identify specific combinations of the optical and acoustic modes resulting in the multipeak structure of BGS in an FMF. The acoustic modes are identified through the relevant the intramodal and intermodal phase-matching conditions, to estimate the BGS, the detailed procedure of which is described below.

2.1. Theoretical background

The GI-FMF used in our experiments supports three spatial optical modes — LP_{01} and the two degenerate LP_{11} modes. The optical mode of the pump and the acoustic mode that it interacts with, are decided by the phase-matching condition given by

$$\beta^{m}_{Pump} + \beta^{n}_{Stokes} = \beta^{s}_{ac}, \tag{1}$$

where β^{m}_{Pump} and β^{n}_{Stokes} represent the propagation constants of the optical modes corresponding to the forward-propagating pump and the backward-propagating Stokes waves respectively, and β^{s}_{ac} is propagation constant of the interacting acoustic mode. The superscripts m, n represent the mode indices of the optical modes while s represents the mode number of the acoustic mode. For the fiber considered in this work, m and n take values either 1 or 2, resulting in two possible cases: (a) $m = n$, corresponding to intramodal SBS and (b) $m \neq n$, corresponding to intermodal SBS. Neglecting damping of the generated acoustic waves, the wave equation satisfied by the longitudinal acoustic modes is given by

$$\nabla^2 u_s + \left(\frac{\Omega^2_{ac}}{V_{ac}(r)^2} - \beta^2_{ac} \right) u_s = 0. \tag{2}$$

The transverse mode profiles of the supported acoustic modes (u_s) are found by solving Eq (2) with the appropriate boundary conditions [9,24]. In Eq. (2), $V_{ac}(r)$ and Ω_{ac} represent the acoustic velocity profile of the fiber and the acoustic angular frequency of the sth acoustic mode respectively. The first term inside the brackets is related to the acoustic propagation constant expressed as $\Omega_{ac}/V_{ac}(r)$, the exact value of which is decided by the effective velocity (V_{eff}) of the supported acoustic mode and its wavelength (Λ) through the relation, $\Omega_{ac} = \frac{2\pi}{\Lambda} V_{eff} = \frac{2\pi}{\Lambda} \frac{V}{n_{ac\_eff}}$; where n_{ac_eff} represents the effective acoustic index of the supported acoustic mode and V represents the velocity of the acoustic wave in the cladding (used here as the reference). In order to find the supported acoustic modes, Eq. (2) is discretized and solved using the finite difference method by casting the difference equations into an eigenvalue equation [9,26]. Eq. (2) is solved independently for intramodal and intermodal interactions by initializing the n_{ac_eff} with the value derived from Eq. (1) for the corresponding interacting modes. The n_{eff} and hence the β^{m}_{Pump} and β^{n}_{Stokes} are found by solving the corresponding wave equation for the electric fields supported by the optical fiber in a similar manner. The effective indices of the acoustic modes are used to calculate the BFS (υ_B) as [20]

$$\upsilon_B = \left(\frac{n^{m}_{eff} + n^{n}_{eff}}{\lambda} \right) \frac{V}{n_{ac\_eff}}, \tag{3}$$

where V is the longitudinal acoustic velocity (6005 m/s) in the cladding, $n^{m,n}_{eff}$ are effective mode indices of optical modes (m, n) and n_{ac_eff} is found by solving Eq. (2). Assuming a Lorentzian lineshape for each of the Brillouin interactions, the overall Brillouin gain spectrum can be written as,

$$g(\upsilon) = \sum_{l} \frac{(\Delta\upsilon_{Bs}/2)^2}{(\upsilon - \upsilon_{Bs})^2 + (\Delta\upsilon_{Bs}/2)^2} \Gamma_l, \tag{4}$$

where $\Delta\upsilon_{Bs}$ is the linewidth contributed by the sth acoustic mode and Γ_s is the overlap integral of the sth acoustic mode and the corresponding phase-matched optical mode. For these simulations, we assume $\Delta\upsilon_{Bs} = 30$ MHz for all modes [27]. We use the mode solver based on finite difference method in MATLAB to calculate all the optical modes and acoustic modes supported by the fiber used for the experiments [26]. We then select the acoustic modes having a large overlap with the optical modes of the fiber to calculate its BGS. This is done systematically for both intermodal and intramodal configurations.

2.2. Simulation results

The refractive index profile of the GI-FMF used in our experiments is shown in Fig. 1a (black curve). The profile clearly indicates a trench-assisted cladding with a graded index core. The acoustic profile of the fiber is also shown (right-y axis) in terms of acoustic velocity $V_{ac}(r)$ [13]. The acoustic velocity is extracted using Eq (5) where the dopant concentration of germanium (Ge) and fluorine (F) are obtained from the given refractive index profile.

$$V_{ac}(r) = V(1 - 7.2 \times 10^{-3} Ge - 2.7 \times 10^{-2} F) \tag{5}$$

The dopant concentrations of Ge and F are extracted using the relation, $n_{optical}(r) = n_{clad}(1 + 10^{-3} Ge - 3.3 \times 10^{-3} F)$ by substituting $n_{optical}(r)$ of the graded core and trench respectively. It is found from the measured $n_{optical}(r)$ that the concentration of Ge is graded from 0–7.3% and the F concentration is constant as 1.8% for the given cladding index of 1.453. The BFS is calculated by substituting the calculated effective index values, $n^{m,n}_{eff}$ and n_{ac_eff} in Eq (3) and is plotted for both the intramodal and intermodal cases in Fig. 1b as a function of the acoustic mode velocity ($V_{eff} = V/n_{ac\_eff}$). Here, the intramodal interaction corresponds to the case when both the pump and Stokes propagate in the LP_{01} mode and the intermodal interaction corresponds to the case when pump and Stokes are paired as LP_{11}-LP_{01} modes respectively. These acoustic mode profiles of symmetric (L_{0s}) and anti-symmetric (L_{1s}) mode groups are also shown with their BFS values (data points shown by a star) in Fig. 1b. It is clear that the higher order acoustic modes correspond to larger BFS values.

Fig. 1c shows the simulated BGS in the intramodal and intermodal cases; the acoustic mode responsible for each peak is also indicated. The BGS is calculated using Eq. (4) by including the overlap area of corresponding acoustic and optical modes for the intramodal and intermodal configurations. From the overlap calculation, it is found that the intramodal BGS is contributed primarily by the L_{0s} acoustic mode group, while intermodal BGS is primarily due to the L_{1s} group, as shown in Fig. 1c (left y-axis) by the blue and red curves respectively. The intermodal interaction with the L_{0s} mode group has negligible gain, as can be seen from the right y-axis of Fig. 1c (green curve). The

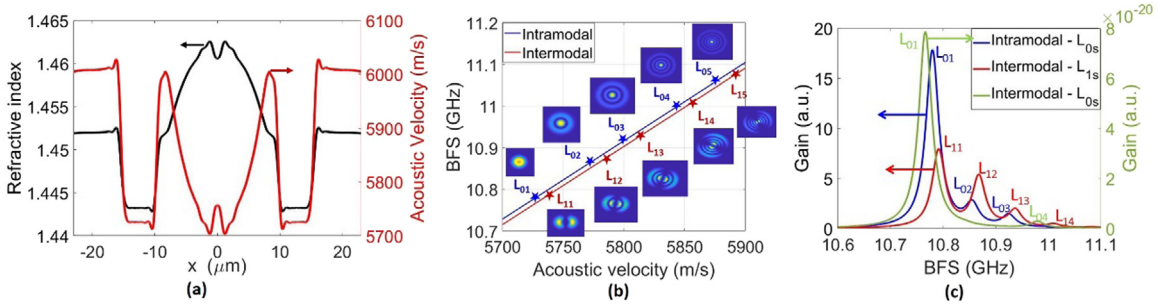

Fig. 1. (a) Refractive index profile of the GI-FMF is shown along with the corresponding acoustic velocity (y-axis on right). (b) BFS with respect to the acoustic velocity of the modes for intramodal and intermodal cases. The acoustic mode profiles are shown as the insets for acoustic velocities corresponding to ten acoustic modes. (c) Calculated BGS for intramodal interaction with the acoustic modes of L_{0s}, intermodal interaction with the acoustic modes of L_{1s}, and intermodal interaction with L_{0s} acoustic modes (on right) y-axis.

SBS gain in the intramodal case is large only for the main peak resulting from SBS interaction involving the fundamental acoustic mode L_{01} and becomes negligible for orders higher than L_{03}. In the intermodal case, SBS gain remains considerably high interactions involving the higher order acoustic modes (L_{12}-L_{14}) and with gain values higher than those in the intramodal case. This difference is due to the overlap between the corresponding modes. Fig. 1c shows that the gain values are significant only for selective sets of acoustic modes — three L_{0s} modes in intramodal case and four L_{1s} modes in intermodal case as shown on left y-axis. The simulated BGS shown in Fig. 1c are compared with the observed experimental BGS data in Section 4. Note that these simulations would represent the generation and interaction of acoustic modes in the self-stimulated configuration, since the influence of an external Stokes radiation propagated in the backward direction in the Brillouin amplifier configuration is not considered. Hence, any experiment intended to reproduce Fig. 1c must be carried out in the self-stimulated configuration.

3. Experimental details

We have used a 1 km long GI-FMF, whose profile is shown in Fig. 1a to measure the BGS experimentally. Since the fiber supports the three spatial modes — LP_{01}, LP_{11a} and LP_{11b}, we have employed both the intramodal and intermodal SBS configurations using the setup shown in Fig. 2a. Our data is based on recording of the beating of the reflected Stokes wave with the input pump. This beat spectrum approach has the advantage of maintaining low input powers such that the BGS can be recorded under unsaturated operating conditions. In Fig. 2a, the pump laser (linewidth-100 kHz) is connected to an isolator to protect it from back-scattered light. The pump power is split using a 50:50 splitter, one of which is launched into a 1-km-long graded index FMF and the second part is used for beating with the SBS-generated Stokes wave. The input to the FMF is amplified using an EDFA, followed by a bandpass filter to eliminate out-of-band amplified spontaneous emission. The amplified pump (P_{pump}) is launched into the FMF using a circulator in two different ways. (a) *Direct-launching mode*: the pump is launched so that it excites only the LP_{01} mode and (b) *Offset-launching mode*: the pump is launched using offset splicing so that both the LP_{01} and LP_{11} modes are excited. The modal profile of launched mode through offset splicing is captured on the camera at the FMF output as shown in Fig. 2b. In both these cases, the Stokes wave is measured only in the fundamental LP_{01} mode as the circulator used in the experiment is based on a single-mode fiber. In our experiments, intermodal measurements correspond to the interaction between the pump in the LP_{11} mode and the Stokes in LP_{01} mode, while intramodal measurements correspond to the case where both pump and Stokes are in the fundamental mode. The reflected Brillouin Stokes power $P_{reflected}$ is extracted using port-3 of the circulator and mixed coherently with the input pump (Pin) using 2×1 coupler, and the combination is allowed to beat on a high-speed photodetector (3 dB bandwidth-10 GHz). The beat spectrum is measured using an electrical spectrum analyzer (ESA) (9 kHz-30 GHz). A variable optical attenuator (VOA) is used to ensure that the input optical power to the detector is below its saturation. All relevant features of BGS are analyzed using the measured beat spectrum.

In order to study intramodal scattering, we carry out a splice between the SMF and FMF with center of the cores of the two fibers aligned, before splicing. In the intermodal case, the input pump is launched through offset splicing such that the modal content is intentionally higher in the higher order LP_{11} mode. The experimentally captured composite mode profile is shown in Fig. 2b. Modal decomposition using the stochastic parallel gradient descent (SPGD) method is carried out to ascertain the proportion of LP_{01} and LP_{11} modes [28]. The pure LP_{01} and degenerate LP_{11a} and LP_{11b} are used as the basis modes for the decomposition shown in Fig. 2b. The reconstructed intensity profile is also shown in Fig. 2b along with the residual intensity error profile. LP_{11} mode is found to have a weight of 60%. Since the degenerate LP_{11a} and LP_{11b} modes have the same effective indices, their BFS values are identical, and they also contribute in the same way to the overlap factor. Thus, the combined weight of 60% is for both LP_{11a} and LP_{11b} modes, and it is challenging to identify their individual contributions in our scalar approach.

The measured spectra in the fundamental mode are shown in Fig. 2c for the intramodal case and in Fig. 2d for the case where the pump is launched in both LP_{01} and LP_{11} modes, resulting in both the intramodal and intermodal contribution. The gain spectra measured for the different values of input pump powers to the FMF are shown in these plots. In the intramodal interaction (Fig. 2c), the number of resolved peaks increases with the pump power, with three peaks appearing in the power range of 4.9–15.8 dBm. The fourth peak is evident for the highest pump power used. Intermodal mixing also results a multipeak structure but with more asymmetrically broadened spectrum and exhibits higher gain for SBS interaction involving higher order acoustic modes. The BFS values of each peak in both Figs. 2c and 2d are indicated by vertical dashed lines. From the experimental BGS spectra, it is clear that the multiple peaks have different gains and the corresponding BFS values are unequally separated. The differences in BFS peak values of BGS are mainly due to higher order acoustic modes, which have a larger overlap with the optical modes. In the next section, numerical simulations are used to fit the observed multi-peak structure in BGS owing to intramodal and intermodal interactions.

4. Fitting of experimental data with numerical simulations

As discussed in Section 2, the multipeak BGS is obtained by assigning different acoustic modes to each peak in both the intramodal and intermodal cases (Fig. 1c). Now, we use the simulated BGS to fit the experimentally observed BGS in the cases of direct-launching and offset-launching.

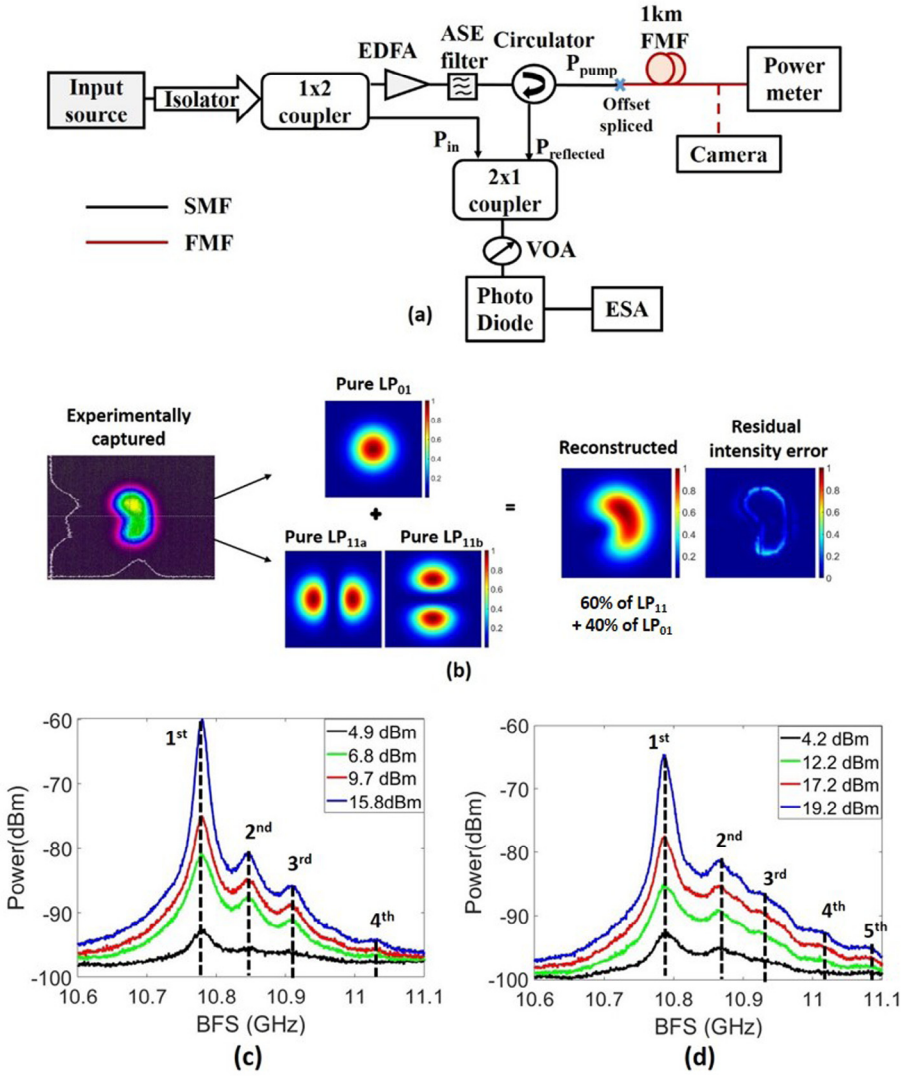

Fig. 2. (a) The schematic of experimental setup to measure BGS is shown, where the beat spectrum of reflected Stokes field with that of the pump is detected. (b) The experimentally captured mode profile is shown as a composition of pure LP_{01} and $LP_{11a/b}$ modes along with the reconstructed mode profile as well as the residual intensity profile. The measured BGS is shown when the input is launched in (c) LP_{01} mode and in (d) composite LP_{01} + LP_{11} mode (40% + 60%) for different input pump power levels.

4.1. Direct-launching

When the pump is launched into a fiber consisting of a center-aligned splicing of SMF to the FMF without any offset, only in the LP_{01} mode of the fiber is excited. As the Stokes wave is also generated predominantly in the LP_{01} mode, the observed BGS results from an intramodal SBS process. The corresponding simulation results in Fig. 1c shows that only the L_{0s} group of acoustic modes contributes to the BGS peaks. The dotted curve in Fig. 3 shows the simulated BGS in the intramodal case. It shows that the three peaks result from three acoustic modes L_{01}, L_{02} and L_{03}. This spectrum should be compared with the BGS obtained from experiments shown by the solid blue line. The frequency corresponding to the three peaks agree well with the predicted values. The experimental curve shows a weak fourth peak at a frequency >11 GHz that does not appear in numerical simulations. One possible reason for this discrepancy may be small variations of the dopant densities along the fiber length, leading to an ambiguity in the estimation of especially higher order acoustic mode.

We assume in simulations that the acoustic profile is uniform along the length of the fiber which may not be the case in the fiber used in the experiment. We have also not considered in the simulations that there may be coupling between the LP_{01} to LP_{11} modes in the intramodal

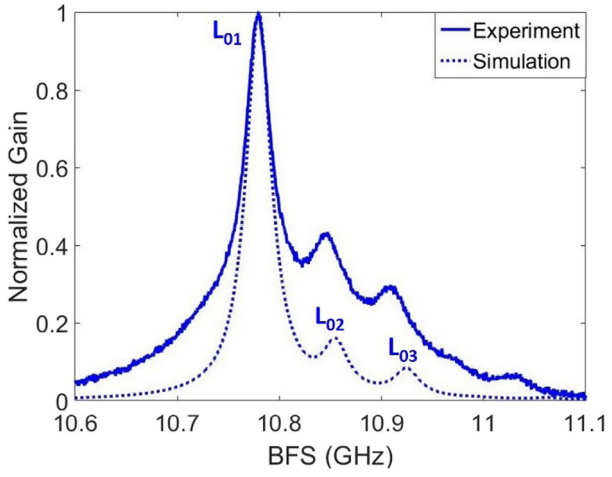

Fig. 3. The simulated and experimental BGS are shown for intramodal case using direct launching.

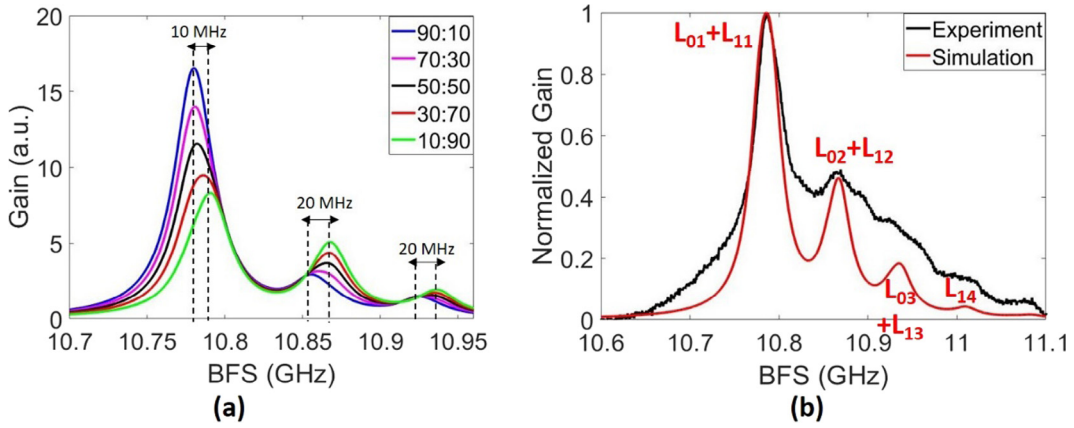

Fig. 4. The simulated and experimental BGS plot is shown for (a) total BGS with different modal weights of intramodal and intermodal, (b) the simulated BGS of 30:70 with experimental BGS of composite pump case. The corresponding acoustic modes are indicated on simulated peaks.

Table 1
Experimental and simulated BFS values for intramodal and intermodal SBS processes.

Intramodal SBS		Intermodal SBS (composite pump case) LP_{01}:30% & LP_{11}:70%	
Experimental BFS (GHz) (f_{exp})	Simulated BFS (GHz) (f_{sim})	Experimental BFS (GHz) (f_{exp})	Simulated BFS (GHz) (f_{sim})
10.78	L_{01} - 10.78	10.79	L_{11} - 10.79
10.85	L_{02} - 10.86	10.87	L_{12} - 10.87
10.91	L_{03} - 10.92	10.93	L_{13} - 10.93
–	–	11.00	L_{14} - 11.01
–	–	11.08	L_{15} - 11.08

case. These two factors may be responsible for the differences seen in Fig. 3. It should also be noted that, when the fundamental optical mode is phase matched with the acoustic L_{01} mode, its phase matching efficiency with higher order acoustic modes may be weaker, which would further need to be considered to achieve an exact match.

4.2. Offset-launching

In case of offset launching, the FMF is spliced with an SMF at slightly off-axis of the fiber core–core alignment. The splicing is done in an active mode where a camera is used to monitor the output of the FMF port to record the excited modal composition in offset position. The launched mode is a composite mode as the modal profile is shown in Fig. 2b. The normalized BGS in this case is calculated by considering the sum of both the intramodal and intermodal cases in order to match with the experimental result shown in Fig. 2d. When input pump excites both LP_{01} and LP_{11} modes, one must consider all possible intermodal and intramodal interactions for a reasonable agreement with the experiments.

The modal weights of individual modes in the composite pump decides the total BGS with slightly shifted BFS values and also the peak gain values. The net BGS, $g(\nu)$ is represented as $ag_{01} + bg_{11}$, where the coefficients 'a' and 'b' represent fractional modal pump power values for LP_{01} and LP_{11} modes with the corresponding gain coefficients g_{01} and g_{11} respectively. Fig. 4a shows the simulated spectra corresponding to the total BGS of the combined intramodal and intermodal cases for five different combinations of a:b – 90:30, 70:30, 50:50, 30:70 and 10:90. It is found that the BGS peaks not only change in amplitude but are also shifted in the frequency depending on the modal weights. The BGS peaks resulting from higher order acoustic modes are shifted by 20 MHz while the main peak is slightly shifted by 10 MHz toward the higher frequency side when the contribution due to intermodal mixing is highest. The gain values decrease for fundamental mode while it increases further for higher-order BFS peaks with an increase in weights of intermodal BGS. This is an interesting aspect of Fig. 4a where the gain value of each mode especially the main peak is significantly tuned by changing the modal composition.

Fig. 4b shows the fitting of experimental data in the intermodal case, where we have both the intramodal and intermodal pump–Stokes pairs. As we have unequal powers in the two pump modes with a larger fraction in the LP_{11} mode, SBS interaction for the intermodal pump–Stokes pair is stronger than for the intramodal pair. The best fit between the experimental data and numerical simulation is corresponds to 70% of pump power in the LP_{11} mode and the remaining 30% in the LP_{01} mode (30:70 excitation ratio). The modal composition fitting in Brillouin process is different from the modal weights extracted from the digital modal decomposition method only by 10%. This specific combination results in a good match between experimentally observed BGS (in black) and the simulated one. The acoustic modes of L_{0s} and L_{1s} groups that contribute to each peak are also indicated in Fig. 4b where L_{0s} corresponds to intramodal case with 30% contribution and L_{1s} to intermodal with 70% contribution to total BGS. The linewidth differences between the experiment and simulation can be attributed to the fact that our simulations assumed that the Brillouin linewidth of each peak is 30 MHz while in reality, this may not be the case [4]. In fact, the linewidth for the various higher order interactions may actually be different. This is explored in further detail in Section 4.3.

The predicted and observed BFS values for intramodal and intermodal cases are tabulated in Table 1 individually. The non-uniformity of the refractive index along the length of the fiber affects the shifts differently because BFS depends on the effective indices linearly for optical modes and inversely for acoustic modes. This behavior of BFS shift can be useful for multiparameter sensing because only the different BFS peaks undergo a different sensitivity to frequency shift owing to changes in the refractive index. Our experimental results agree well theoretical predictions and the multipeak BFS shows applicability for multiparameter distributed sensors.

4.3. Lorentzian fitting to multipeak BGS

We now proceed to carry out a more careful fit of the experimental BGS of composite pump case by allowing different linewidths for its

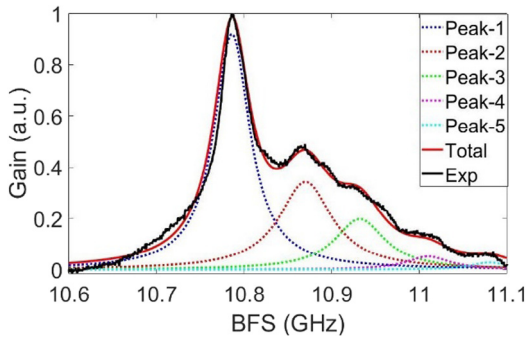

Fig. 5. The multipeak Lorentzian fit is shown with experimental BGS for intermodal case.

Table 2
Fitted values of BFS and linewidth of each Lorentzian peak.

Peak no	BFS (GHz)	Width (MHz)
1	10.79	50
2	10.87	74
3	10.93	70
4	11.01	60
5	11.08	50

each peak. The linewidth ($\Delta\nu_B$) is expressed as $\beta_{ac}^2\gamma/2\pi$ where β_{ac} is the propagation constant of acoustic modes and γ is the damping parameter of acoustic phonons [29]. This expression shows why the linewidth of acoustic modes can be different depending on the specific intramodal and intermodal interactions. Fig. 5 shows how the experimental BGS can be fitted by using a Lorentzian curve for each peak such that the sum of the five Lorentzian functions results in the observed BGS. Table 2 shows the peak position (BFS) and the linewidth of each Lorentzian. It is found that the observed BGS is the sum of the intramodal and intermodal gains of higher order acoustic modes leading to different linewidths. The overlapping of intramodal and intermodal gains gives the asymmetric spectral broadening in the observed BGS, which could not be explained in Fig. 4 where the linewidth were presumed to be identical for all the peaks. The multipeak Lorentzian fit provides the BFS value as well as the linewidth of each gain peak.

We note that the multipeak BGS depends selectively on several pairs of optical and acoustic modes that depend on the pump and acoustic mode groups (radially symmetric versus anti-symmetric) and orders (fundamental or higher order). The correct identification of multiple acoustic modes of different mode groups and of mode orders provides the values of BFS shifts with higher accuracy. The modal content of pump mode gives an additional control on choosing the optical and acoustic mode pairs which are useful in simultaneous and discriminated measurement of the sensing parameters.

5. Conclusions

In this work, we have discussed the origin of a multipeak structure in the BGS measured for a graded-index few-mode fiber. We used numerical simulation to find that the radially symmetric acoustic mode group (L_{0s}) is primarily responsible for intramodal interaction when both the pump and Stokes waves propagate in the fundamental LP_{01} mode. In contrast, intermodal interaction occurring when the pump is in the LP_{11} mode and the Stokes is in the LP_{01} mode is mediated through the radially anti-symmetric L_{1s} mode. We obtained the predicted BGS through numerical simulations after including both intramodal and intermodal processes and identified all prominent acousto-optic interactions that contributes to the BGS. We used our numerical predictions to explain the multipeak structure observed experimentally. In addition to the interacting modes, we found that the modal weights of the launched pump power play a significant role in forming the composite gain spectrum. By tuning the modal weights where LP_{01} is reducing and LP_{11} is increasing, the main peak shifts by approximately 10 MHz with the reduced gain value and other higher order peaks shift by 20 MHz with increase in its gain value. For our specific experiment, we identified the modal composition to be 70% (LP_{11} mode) and 30% (LP_{01} mode). We also fitted the observed BGS with five Lorentzian spectra of different widths and found that the width of each peak in BGS spectrum is also decided by the interacting acoustic modes. The precise methodology presented in this paper to identify the specific acoustic modes based on the modal weights of the pump along with the correct identification of the linewidth may find several applications including multi-parameter distributed sensing.

Declaration of competing interest

The authors declare that they have no known competing financial interests or personal relationships that could have appeared to influence the work reported in this paper.

Acknowledgment

The authors acknowledge the funding support from Ministry of Electronics and information technology (MEITY), India and SPARC funding of MHRD, Govt. of India. Suchita acknowledges Dr. Shahna Haneef for providing the mode solver and Dr. Karamdeep Singh for doing the SPGD based digital modal decomposition.

References

[1] E.P. Ippen, R.H. Stolen, Stimulated Brillouin scattering in optical fibers, Appl. Phys. Lett. 21 (1972) 539–541, https://doi.org/10.1063/1.1654249.
[2] V.R. Supradeepa, Stimulated Brillouin scattering thresholds in optical fibers for lasers linewidth broadened with noise, Opt. Express 21 (2013) 4677–4687, https://doi.org/10.1364/oe.21.004677.
[3] S. Preußler, A. Wiatrek, K. Jamshidi, T. Schneider, Brillouin scattering gain bandwidth reduction down to 3.4MHz, Opt. Express 19 (2011) 8565–8570, https://doi.org/10.1364/oe.19.008565.
[4] G.P. Agrawal, Nonlinear Fiber Optics, sixth ed., Academic Press, 2019.
[5] D.A. Fishman, J.A. Nagel, Degradations due to stimulated Brillouin scattering in multigigabit intensity-modulated fiber-optic systems, J. Lightwave Technol. 11 (1993) 1721–1728, https://doi.org/10.1109/50.251167.
[6] N. Ohkawa, Y. Hayashi, Reduction of bit error rate performance deterioration caused by stimulated brillouin scattering in high-power CPFSK coherent optical transmission systems, Electron. Lett. 30 (1994) 515–516, https://doi.org/10.1049/el:19940369.
[7] Y. Aoki, K. Tajima, I. Mito, Input power limits of single-mode optical fibers due to stimulated Brillouin scattering in optical communication systems, J. Lightwave Technol. 6 (1988) 710–719, https://doi.org/10.1109/50.4057.
[8] Y. Jeong, J. Nilsson, J.K. Sahu, D.N. Payne, R. Horley, L.M.B. Hickey, P.W. Turner, Power scaling of single-frequency ytterbium-doped fiber master-oscillator power-amplifier sources up to 500 W, IEEE J. Sel. Top. Quantum Electron. 13 (2007) 546–550, https://doi.org/10.1109/JSTQE.2007.896639.
[9] M.-J. Li, X. Chen, J. Wang, S. Gray, A. Liu, J.A. Demeritt, A.B. Ruffin, A.M. Crowley, D.T. Walton, L.A. Zenteno, Al/ge co-doped large mode area fiber with high SBS threshold, Opt. Express 15 (2007) 8290–8299, https://doi.org/10.1364/oe.15.008290.
[10] L. Dong, Formulation of a complex mode solver for arbitrary circular acoustic waveguides, J. Lightwave Technol. 28 (2010) 3162–3175, https://doi.org/10.1109/JLT.2010.2078488.
[11] X. Bao, L. Chen, Recent progress in distributed fiber optic sensors, Sensors 12 (2012) 8601–8639, https://doi.org/10.3390/s120708601.
[12] L. Thévenaz, Review and progress in distributed fiber sensing, OSA optical fiber sensors (OFS), ThC1 (2006) https://doi.org/10.1364/OFS.2006.ThC1.
[13] P. Dragic, J. Ballato, A brief review of specialty optical fibers for Brillouin-scattering-based distributed sensors, Appl. Sci. 8 (2018) 1996, 1-24. https://doi.org/10.3390/app8101996.
[14] L. Tartara, C. Codemard, J.N. Maran, R. Cherif, M. Zghal, Full modal analysis of the Brillouin gain spectrum of an optical fiber, Opt. Commun. 282 (2009) 2431–2436, https://doi.org/10.1016/j.optcom.2009.03.012.
[15] An Li, Yifei Wang, Jian Fang, Ming-Jun Li, Byoung Yoon Kim, William Shieh, Few-mode fiber multi-parameter sensor with distributed temperature and strain discrimination, Opt. Lett. 40 (2015) 1488–1491, https://doi.org/10.1364/OL.40.001488.

[16] M. Chen, A. Masoudi, F. Parmigiani, G. Brambilla, Distributed acoustic sensor based on a two-mode fiber, Opt. Express 26 (2018) 25399–25407, https://doi.org/10.1364/oe.26.025399.

[17] J. Fang, G. Milione, J. Stone, G. Peng, M.-J. Li, E. Ip, Y. Li, P.N. Ji, Y.-K. Huang, M.-F. Huang, S. Murakami, W. Shieh, T. Wang, Multi-parameter distributed fiber sensing with higher-order optical and acoustic modes, Opt. Lett. 44 (2019) 1096–1099, https://doi.org/10.1364/ol.44.001096.

[18] Nori Shibata, Katsunari Okamoto, Yuji Azuma, Longitudinal acoustic modes and Brillouin-gain spectra for GeO2-doped-core single-mode fibers, J. Opt. Soc. Amer. B 6 (1989) 1167–1174, https://doi.org/10.1364/JOSAB.6.001167.

[19] Sergey V. Tsvetkov, Maxim M. Khudyakov, Alexey S. Lobanov, Denis S. Lipatov, Mikhail M. Bubnov, Alexey N. Guryanov, SBS Gain suppression in a passive single-mode optical fiber by the multi-mode acoustic waveguide design, J. Lightw. Technol. 392 (2021) 592–599, https://doi.org/10.1109/JLT.2020.3031726.

[20] K.Y. Song, Y.H. Kim, Characterization of stimulated Brillouin scattering in a few-mode fiber, Opt. Lett. 38 (2013) 4841–4844, https://doi.org/10.1364/ol.38.004841.

[21] W. Chen, G. Hu, F. Liu, F. Wang, C. Song, X. Li, Y. Yu, Threshold for stimulated Brillouin scattering in few-mode fibers, Appl. Opt. 58 (2019) 4105–4110, https://doi.org/10.1364/AO.58.004105.

[22] A. Minardo, R. Bernini, L. Zeni, Experimental and numerical study on stimulated Brillouin scattering in a graded-index multimode fiber, Opt. Express 22 (2014) 17480, https://doi.org/10.1364/oe.22.017480.

[23] K.Y. Song, Y.H. Kim, B.Y. Kim, Intermodal stimulated Brillouin scattering in two-mode fibers, Opt. Lett. 38 (2013) 1805–1807, https://doi.org/10.1364/ol.38.001805.

[24] Y.S. Mamdem, X. Pheron, F. Taillade, Y. Jaouën, R. Gabet, V. Lanticq, G. Moreau, R. Edf, I. Telecom, T. Paristech, L.H. Curien, Two-dimensional FEM analysis of Brillouin gain spectra in acoustic guiding and antiguiding single mode optical fibers, Comsol Conf. 1 (2010) 1–7.

[25] S. Dasgupta, F. Poletti, S. Liu, P. Petropoulos, D.J. Richardson, L. Grüner-Nielsen, S. Herstrøm, Modeling Brillouin gain spectrum of solid and microstructured optical fibers using a finite element method, J. Lightwave Technol. 29 (2011) 22–30, https://doi.org/10.1109/JLT.2010.2091106.

[26] S.M. Haneef, P.P. Prashanth, B. Venkitesh, D. Srinivasan, Modeling stimulated brillouin scattering in LEAF using finite difference method, in: OSA Photonics 2014: 12th International Conference on Fiber Optics and Photonics, 2014, p. S5A.39, https://doi.org/10.1364/PHOTONICS.2014.S5A.39.

[27] Marc Nikl'es, Luc Thévenaz, Philippe A. Robert, Brillouin gain spectrum characterization in single-mode optical fibers, J. Lightw. Technol. 15 (1997) 1842–1851, https://doi.org/10.1109/50.633570.

[28] K. Singh, P. Sharma, B. Srinivasan, R.D. Koilpillai, D. Venkitesh, Digital modal decomposition based on stochastic parallel gradient descent algorithm and its validation, in: Conf. Lasers Electro-Optics Pacific Rim, CLEO-PR 2020 - Proc, 2020, https://doi.org/10.1364/CLEOPR.2020.P2_19.

[29] R.W. Boyd, Nonlinear Optics, second ed., Academic Press, 2003.